# An adaptive coded aperture imager: building, testing and trialing a super-resolving terrestrial demonstrator

Christopher W. Slinger[1]*, Charlotte R. Bennett[‡], Gavin Dyer[§], Kevin Gilholm[‡], Neil Gordon, David Huckridge, Mark McNie[‡], Richard W. Penney[‡], Ian K. Proudler, Kevin Rice[§], Kevin D. Ridley, Lee Russell[‡], Geoffrey D. de Villiers, Philip J. Watson[‡]

Malvern Innovations Ltd, The Elms Courtyard, Bromesberrow, Herefordshire HR8 1RZ, UK
[‡]QinetiQ Malvern, St Andrews Road, Great Malvern, Worcestershire, WR14 3PS, UK;
[§]ISR Systems, Goodrich Corp., Westford, MA.

## ABSTRACT

There is an increasingly important requirement for day and night, wide field of view imaging and tracking for both imaging and sensing applications. Applications include military, security and remote sensing. We describe the development of a proof of concept demonstrator of an adaptive coded-aperture imager operating in the mid-wave infra-red to address these requirements. This consists of a coded-aperture mask, a set of optics and a 4k x 4k focal plane array (FPA). This system can produce images with a resolution better than that achieved by the detector pixel itself (i.e. super-resolution) by combining multiple frames of data recorded with different coded-aperture mask patterns. This super-resolution capability has been demonstrated both in the laboratory and in imaging of real-world scenes, the highest resolution achieved being ½ the FPA pixel pitch. The resolution for this configuration is currently limited by vibration and theoretically ¼ pixel pitch should be possible. Comparisons have been made between conventional and ACAI solutions to these requirements and show significant advantages in size, weight and cost for the ACAI approach.

**Keywords:** Coded-aperture imaging, computational optics, optical design, persistent surveillance.

## 1. INTRODUCTION

There is an increasingly important requirement for day and night, wide field of view imaging and tracking for both imaging and sensing applications. Applications include military, security and remote sensing. In this paper we describe the development of a proof of concept demonstrator of an adaptive coded-aperture imager operating in the mid-wave infra-red to address these requirements. In this paper we describe a system that consists of a coded-aperture mask, a set of optics and a 4k x 4k focal plane array (FPA). A brief overview of adaptive coded aperture imaging (ACAI) is given in section 1. The equipment built is described in section 2 and data processing in section 3. Results of experiments and trials are given in section 4 and comparisons of a potential deployable ACAI sensor compared with conventional approaches in section 5. Conclusions and way forward are given in section 6.

### 1.1 The adaptive coded aperture imaging concept

Coded aperture imaging has been used extensively at γ-ray and X-ray wavelengths, where conventional techniques, based on refractive and reflective optics, are impractical [1,3]. CAI works by coding optical wavefronts from a scene using a patterned aperture (called a mask), detecting the resulting intensity distribution, then using digital signal processing to reconstruct an image of the scene. An example is the NASA Swift satellite Burst Array Telescope (BAT) camera [4]. Launched in November 2004, the system uses a coded aperture system to locate cosmological γ-ray bursts.

[1] * chris.slinger@malverinnovations.com; phone +44 *+44 1531 651 244, www.malverninnovations.com*

Unconventional Imaging, Wavefront Sensing, and Adaptive Coded Aperture Imaging and Non-Imaging Sensor Systems, edited by Jean J. Dolne, Thomas J. Karr, Victor L. Gamiz, Stanley Rogers, David P. Casasent, Proc. of SPIE Vol. 8165, 816511 · © 2011 SPIE · CCC code: 0277-786X/11/$18 · doi: 10.1117/12.895435

CAI is one example of computational imaging (CI) [5]. Recent advances in optical hardware, image processing algorithms and the availability of low cost, abundant digital signal processing (DSP) have stimulated research in CI, particularly for applications where more conventional imaging approaches have been found to be inadequate in some way. Application of CAI to longer wavelengths (for example, visible and infrared wavelengths) is one example of CI, where the availability of reconfigurable coding mask technologies permits a novel variant of CAI known as adaptive coded aperture imaging (ACAI). The basic concept is shown in Fig. 1.

The use of an adaptive mask increases flexibility and introduces the possibility of new modes of operation [5]. One of these involves the combination of a reconfigurable mask with conventional optical elements. These elements produce a more compact point spread function (PSF) compared to an imager that uses just a coded-aperture, which results in large improvements in signal to noise ratio (SNR) [6]. Using a mask allows one to apply CI to correct for aberrations in the optical elements, which means that these elements can be simpler, lighter and cheaper than those of an equivalent conventional imager. In addition, by combining multiple frames of data, each recorded with a different mask pattern, it is possible to produce super-resolved images: images with a resolution smaller than the pixel pitch of the detector [7].

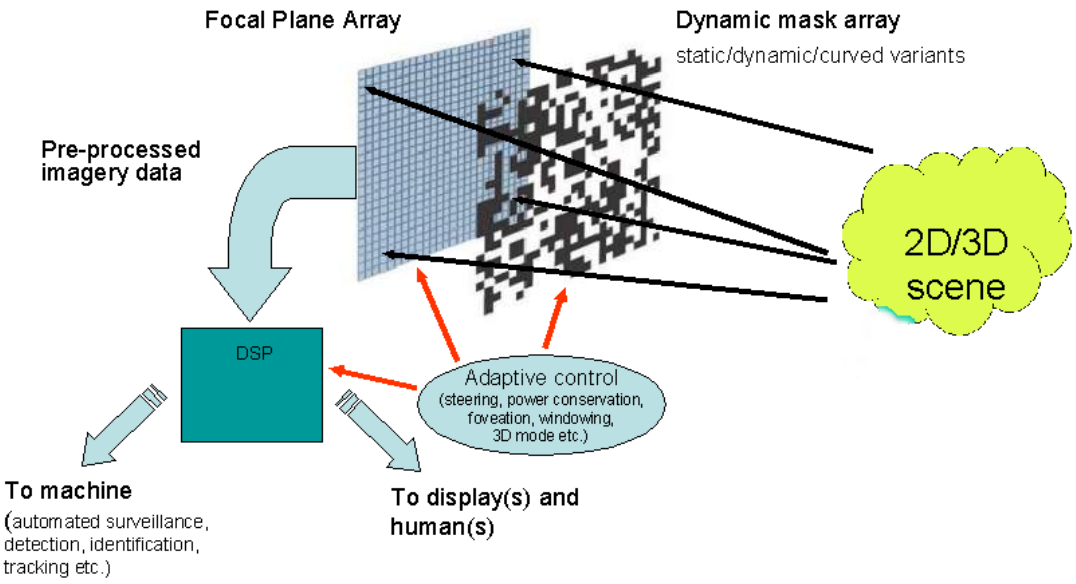


Fig. 1. The basic concept of adaptive coded aperture imaging.

### 1.2 Persistent Wide Area Surveillance (PWAS)

A typical Persistent Wide Area Surveillance application requires a high-resolution, wide field-of-regard system, with a tracking capability in a format which provides realistic size weight and power budget. In order to meet these requirements an ACAI system was designed to provide sub-pixel imaging and tracking performance. Details of the design process have been published elsewhere [21]. The system was based around the detector array with the largest available format [8] (4k x 4k) from Raytheon Vision Systems (RVS). Super-resolved images from this detector will therefore exceed the resolution of any known conventional MWIR system with the same field of view. A major component of the technology is the reconfigurable mask. This has to meet a number of challenging requirements: a large physical aperture, fast switching, operation in the mid-wave infrared etc. The solution adopted is based on a large array of Fabry-Pérot shutters using MOEMS technology [10] as described in a companion paper [23]. By adjusting the coatings on the shutters it was possible to achieve good performance of the shutters (> 90% transmission in the on-state and less than 10% transmission in the off-state) over a 0.5 μm waveband.

## 2. ACAI TERRESTRIAL DEMONSTRATOR

### 2.1 Overview

An initial demonstrator system has been produced to investigate whether the potential benefits of an ACAI system can be realized in a practical system. An overview of the ACAI system is illustrated in figure 2. The basic system looks similar to a conventional system with optics concentrating the radiation onto a large format detector but with the addition of an adaptive mask and the use of signal processing to recover the image. The figure also shows the calibration equipment which consists of a collimator and a mirror in a precision gimbal mount. This calibration process measured the response of the system to a point source to give the point spread function (PSF) of the system. The use of a mirror also allowed the system to quickly switch from calibration to outside imaging.

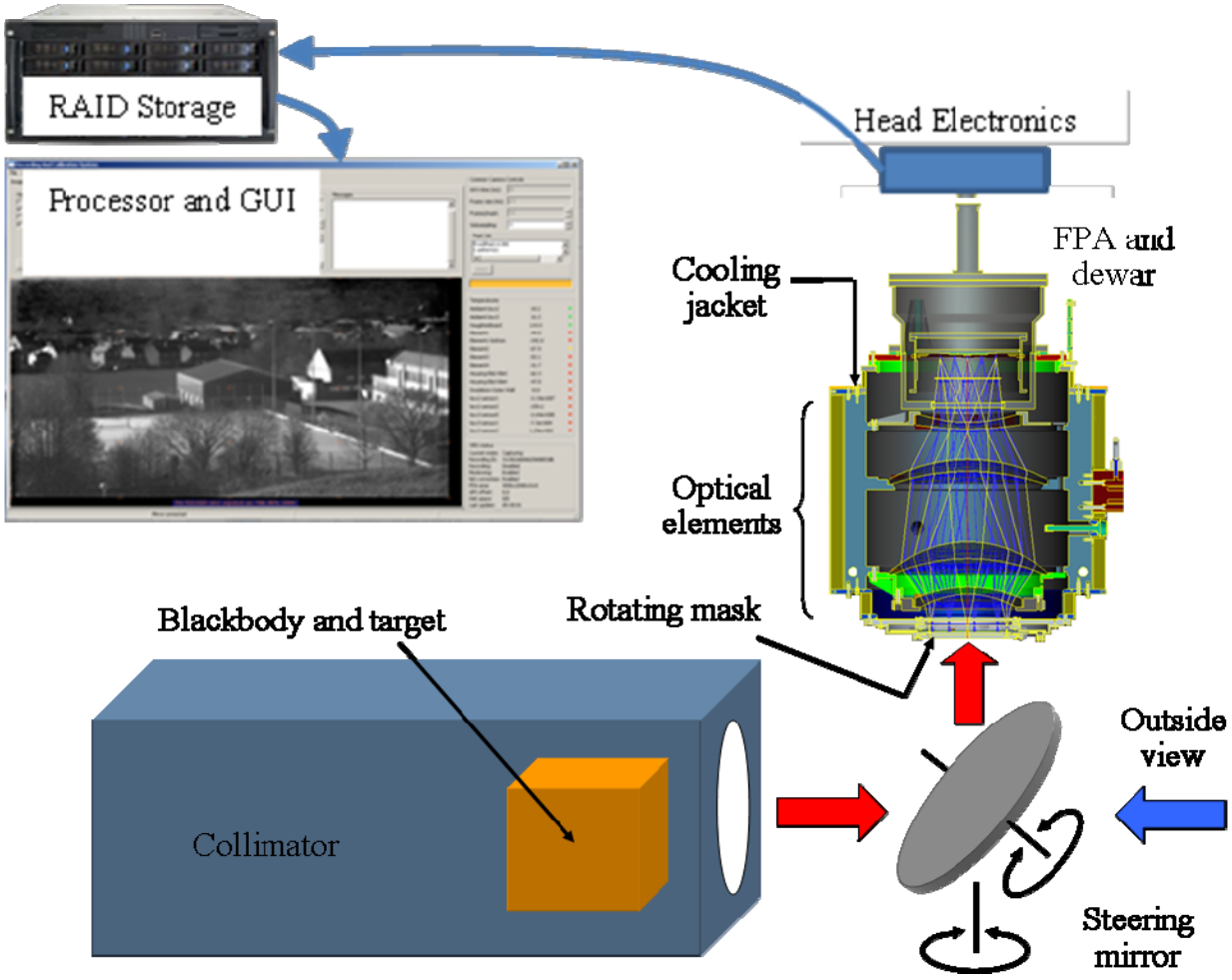


Fig. 2. Overview of the ACAI system including the calibration equipment

### 2.2 The optics

In a conventional system, the optical system is designed to give as good a focus as possible over the field of view. In the ACAI system however concentration is only required to achieve a sufficient signal to noise ratio. The present system was designed to spread the PSFs over around 3 pixels diameter. In addition, the system was designed to minimize the

variation of the PSF with field angle, wavelength and the temperature of the optics. In principle, the variation of the PSF with field position can be removed as part of the processing by measuring the PSF as a function of field angle. However, it was decided to minimize the need for long calibration runs by aiming for the isoplanatic regions to have a width of at least 1 degree. A complete set of the figures of merit are defined in table 1 below and more details of this unconventional optical design process are discussed in reference [21]. The optical layout of the system is shown in figure 3.

A key decision in the optical design process was where to locate the adaptive mask. In the present design, the mask is positioned at the input aperture of the optics. This has the advantages that the radiation from each point in the scene is modulated by the whole mask (which will reduce the angular variation of the PSFs) and easy access to the mask. However, it has the disadvantage that efficient cold shielding of the focal plane array is not possible (see figure 3). It was therefore necessary to cool the optics so that stray radiation from the side walls is not detected. A cooling jacket was designed which used a freezing solution of $CO_2$ in iso-propyl alcohol (IPA) to maintain the optics at a steady temperature of around -80C.

| Number | Purpose | Definition |
|---|---|---|
| M1 | Figure of merit to ensure that most of the PSF is concentrated into a region less than *r* pixels across over the whole field of view. | $M1(r)=\dfrac{\sum_{i,j} PSF\left(i^2+j^2<r^2\right)}{\sum_{i,j} PSF(i,j)}$ |
| M2 | Figure of merit to minimize the variation of the PSF across the field of view i.e. to maximize the isoplanatic field. | $M2(\phi)=\sum_{i,j}\left\|PSF(i,j;\phi)-PSF(i,j;\phi+\Delta\phi)\right\|$ |
| M3 | Figure of merit to minimize the variation of the PSF across the spectral bandwidth of the imager (3.6 – 4.1 μm). | $M3=\dfrac{1}{N}\sum_{n=1}^{N}\sum_{i,j}\left\|PSF(i,j;\lambda_n)-PSF(i,j;\lambda_0)\right\|$ |
| M4 | Figure of merit to minimize the variation of the PSF with the temperature of the optics. The temperature of the optics was controlled to within ±1 K. | $M4=\max\left[\sum_{i,j}\left\|PSF(i,j;T_n)-PSF(i,j;T_0)\right\|\right]$ |

Table 1: Definition of the optimization parameters which were used to ensure a high signal to noise (M1) and to minimize the variation of the PSF with field angle (M2), wavelength (M3) and optics temperature (M4).

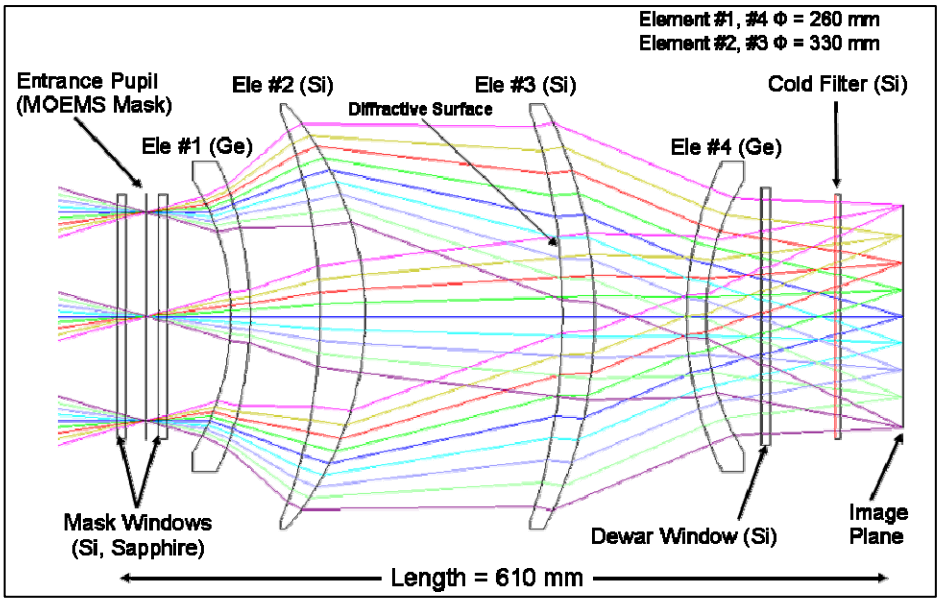


Fig. 3. The optical layout of the ACAI system. The mask is positioned outside the optics at the entrance pupil. This design has the disadvantage that efficient cold shielding of the detector is not possible within the dewar.

### 2.3 Adaptive mask

An adaptive mask consisting of an addressable array of micro shutters based on MOEMS technology is being developed for ACAI applications [23]. This will allow fast switching of a set of mask patterns without any macroscopic moving parts. However, the present experiments used a simpler (but less convenient) approach based on rotating a fixed mask to a set of fixed positions. The fixed mask which was used is shown in figure 4 and consists of a random pattern of 2 cm × 2 cm apertures which were produced by evaporating gold on a silicon substrate. The size of the apertures was chosen to both simulate the capabilities of the MOEMS mask and to provide the correct diffractive characteristics. The rotation mount allows one to choose any of 24 possible positions. This gives sufficient variation of PSFs to achieve sub-pixel resolution to the required level.

Fig.4. The fixed mask in the rotation stage. This could be rotated to a set of up to 24 fixed positions.

### 2.4 Detector

The detector was based on 4k x 4k focal plane array from Raytheon Vision Systems, figure 5. This was mounted in a custom dewar which included a cooled filter to limit the radiation to the bandwidth of the system (3.6 – 4.1 μm). The

central 4k × 2k region was selected and the output was recorded in a RAID array. This was able to record full frame data at the maximum frame rate of the system. The detector was cooled with a pulse tube cooler driven with an air-cooled compressor.

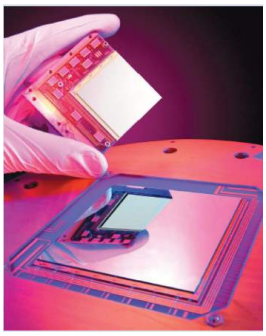

Fig. 5. Photograph of 4k x 4k Raytheon FPA (lower device). Device in the hand is a 2k x 2k FPA, for comparison. Image from Raytheon Vision Systems.

### 2.5 Calibration

The system was calibrated by measuring the output generated by a point source as a function of position across the field of view. A collimator was used to generate a point source at the focal position of the system and the precision gimbals were used to scan the point source to an array of positions across the optical field of view. The PSF contains significant sub-pixel detail and hence the measured PSF will depend on the alignment of the point source with the detector array.

This sub-pixel detail can be revealed by scanning the PSF across a sub-pixel grid. In practice, the PSF was measured over an 8×8 grid and these images can be interlaced to generate some sub-pixel information, figure 6. These interlaced PSFs are used in the sub-pixel algorithms as discussed in section3.2.

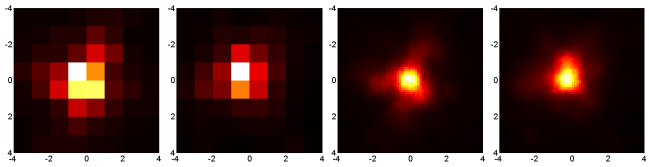

Fig. 6. Left: FPA images of PSF for two mask rotation positions. Right: Corresponding interlaced 8x8 scan of PSFs showing sub-pixel structure

Non-uniformity correction for the detector was achieved by having two temperature controlled black body plates on either side of the mirror. These plates filled the field of view of the sensor and were set to two reference temperatures.

### 2.6 Assembly

Figure 7 shows the completed assembly together with the precision mirror. The cooling jacket was fitted with a filler funnel at the top which greatly reduced the frequency of topping up the $CO_2$ pellets for cooling. The detector head electronics is in the box on top of the assembly, the mirror sits underneath the optics. The mirror was used to switch between the two non uniformity correction reference plates, the collimator for calibration and the window to view outside.

(a)

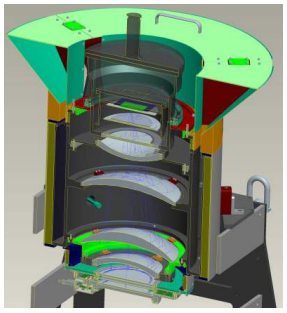

(b)

Fig. 7. (a) This shows the built ACAI system as described in Fig. 2 in the lab showing the optical assembly with cooling jacket, the precision mirror, the detector and the detector head electronics. (b) shows the internal mounting of the optical elements and a cross section of the cooling jacket.

# 3. DATA PROCESSING

## 3.1 Processing for tracking

The primary purpose of the system is to carry out tracking of multiple moving targets. The tracking is Bayesian in nature and is based on correlation with the system point-spread function.

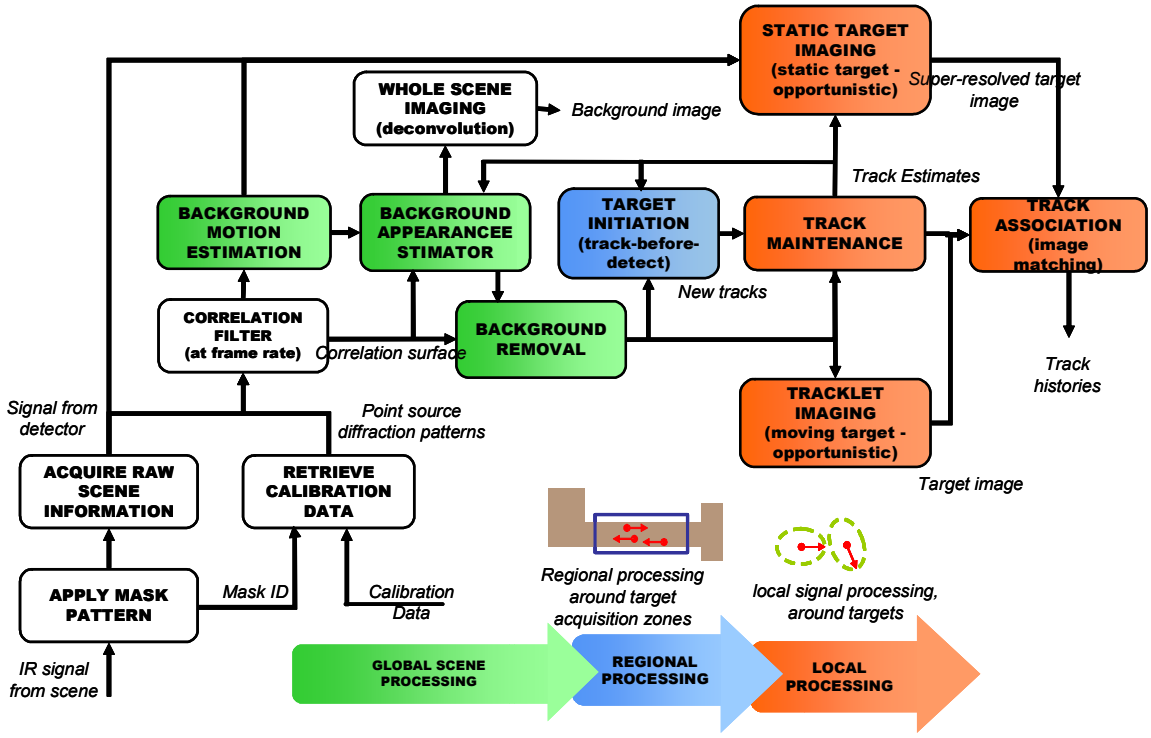


Figure 8 The overall processing scheme

The overall scheme is shown in figure 8. A key point to note is that the tracking is performed on the data after it has been correlated with the system point-spread function. This avoids the presence of significant artefacts in the data which would arise if one were to attempt to deconvolve the point-spread function from the data. In [20] it is shown that it is beneficial to use the correlated data from a likelihood perspective.

The actual tracking process used involves particle filters rather than the conventional Kalman filter due to the non_Gaussian nature of the noise.

### 3.2 Processing for super-resolution

The super-resolution processing can either be carried out in the spatial domain (see [9]) or the Fourier domain (see [13]).. In both of these approaches we need the system point-spread function recorded at sub-pixel displacements of its center., as shown in figure 6. We will give a brief description of the spatial domain process, in one dimension for simplicity.

By using multiple mask patterns in the super-resolution process we are essentially trying to solve a set of simultaneous integral equations of the form

$$g_n^{(m)} = \int \Phi_m(n,x) f(x) dx + noise, \qquad n = 1, \cdots, N$$

Here $g$ corresponds to the data and $f$ to the scene we wish to reconstruct. The indices $n$ and $m$ label the $n$th component of the data vector and the particular mask pattern used respectively.

These integral equations, after the integrals have been discretised, can be grouped together to form a large matrix equation, which is solved using a pseudo-inverse or some other regularization method such as Tikhonov regularization, to cope with the inversion instability caused by the noise.

For the two-dimensional problem the same approach can be taken, after first mapping the two dimensions onto one using, for example, a lexicographic mapping.

The function Φ in the two-dimensional case is the interlaced point-spread function as in figure 6.

If the point-spread function does not vary too greatly over a sufficiently large region (say 100x100 pixels) then the problem can be viewed as a deconvolution and Fourier domain methods can be used as in [13].

In order for these methods to function well it is essential that the point-spread functions for different mask patterns be as linearly independent as possible. This ensures that by changing the mask pattern one gains new information about the sub-pixel structure of the image.

## 4. RESULTS

### 4.1 Super-Resolution Experiments

After assembling the system, a short program of trials and tests were arranged. Initial results were obtained on the sub-pixel performance of the system for both inside and outside scenes, and tracking of both simulated vehicles and dismounts. Figure 9 shows the scene outside the lab before any processing. Although this image looks reasonable, there is some blurring on the pixel scale caused by the extended psf generated by the optics. This blurring can be removed with super resolution processing.


Fig. 9. View from lab taken using the system, prior to super-resolution. This single frame image shows the full 4096×2048 scene.

Figure 10 shows a spoke target in the collimator shown before and after processing. The red circle shows the position where the spoke features are half pixel and demonstrates that sub-pixel imaging can be achieved with the system at all angles. Figure 11 shows the results of repeating this experiment on a spoke resolution target in an outside scene. This again shows that the resolution can be improved to around ½ pixel. This would be equivalent to a 8192×4096 element array. Finally, the super resolution algorithm was applied to features in the scene and figure 12 shows an example of this.

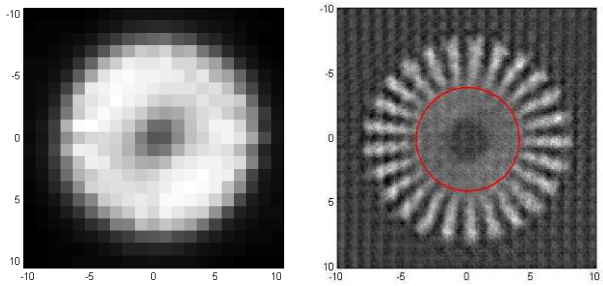

Fig. 10. Result for a spoke target inside the collimator with a temperature difference of 80 K. Left: FPA image. Right: super-resolution result using 16 mask positions; the circle shows half-pixel resolution. The scale is in pixels.

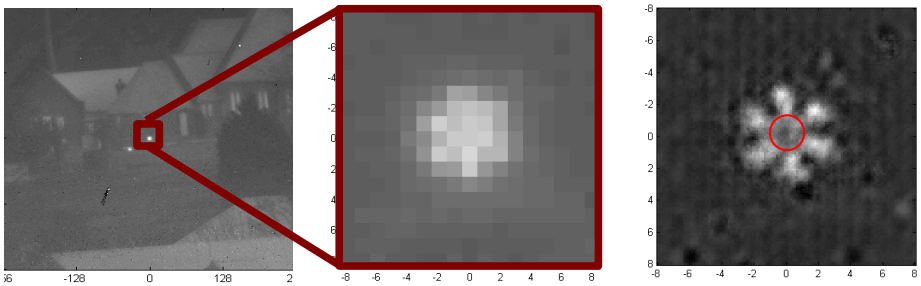

Fig. 11. Result for a spoke target (33 K above ambient) outside of the lab at a distance of 600 m. Left: 512×512 section of image. Middle: Raw FPA image of spoke target showing blurring. Right: super-resolution result using 8 mask positions; the circle shows half-pixel resolution. In both cases, the scale is in pixels.

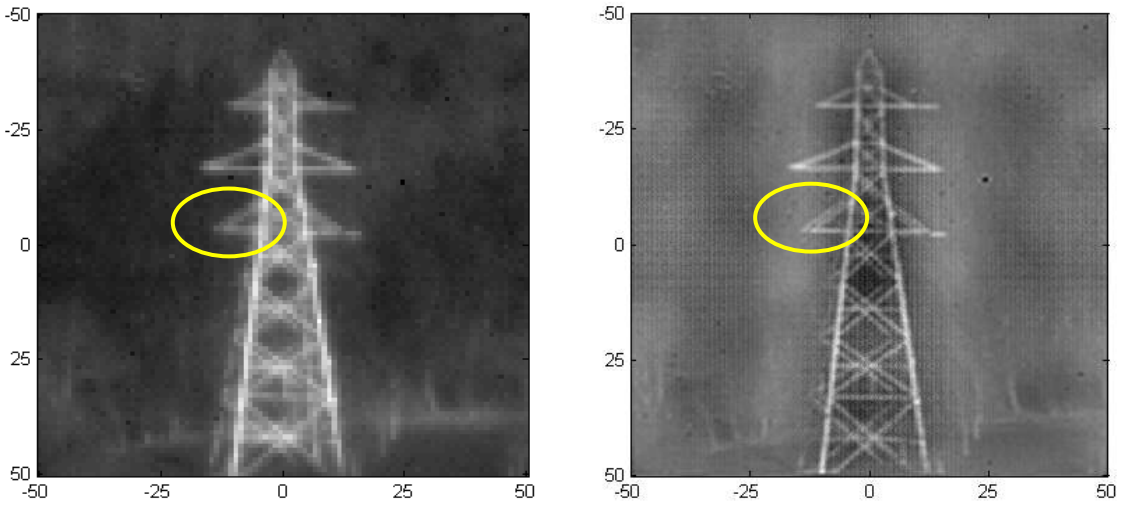

(a) (b)

Fig. 12. A pylon at 4 km showing the image before (a) and after (b) processing. The improved resolution in the processed image can be seen in the sharper struts and the ability to resolve two close struts in the encircled region.

The initial results with this system show that it has been possible to achieve around ½ pixel resolution. However, modeling the system showed that it should be possible to achieve a resolution of ¼ pixel. It is believed that there are a number of factors that are presently limiting the achievable resolution of this experimental system. One of these is due to a relatively high level of vibration that was found to couple to the detector from the pulse tube cooler. This vibration had an amplitude of ½ pixel amplitude and we believe that this can be significantly reduced by modifying the cooler interface or using a different cryocooler technology.

### 4.2 Tracking experiments

Figure 13 – Pictures of the laser tracker board left - close up, right - as seen from the laboratory

One of the objectives of this work was to demonstrate that the system was suitable for tracking vehicles from an altitude of 20 km. Tracking performance at realistic scales was difficult to demonstrate as the system was a laboratory based sensor with a horizontal view. A scaled road scene was drawn on a large board using paints with different infrared properties so that they would show up on an infrared camera. Figure 13 shows a close up of the tracker board as well as the view from the sensor. Vehicles were simulated by projecting a set of up to four infrared laser spots on to the tracker board. The positions of the spots could be moved across the board using computer controlled mirrors. A set of scenarios were programmed which generated realistic vehicle motion and used appropriate spot sizes.

The sensor output was recorded and analyzed using the process described in section 3.1. It was possible to successfully track the simulated vehicles for a wide range of scenarios which included vehicles crossing and overtaking.

## 5. COMPARISON WITH A CONVENTIONAL SYSTEM

To enable size and weight comparisons between sensor system based on ACAI and conventional approaches to a PWAS mission – wide FOV, high resolution, high fidelity tracking, long range – outline designs of two optical systems have been produced. The first design was for a wide FOV optic with an ACAI mask situated inside the optics figure 14a, this approach gives greater freedom to the optics design and allows for efficient detector cold shielding thereby avoiding the need to cool the optics to <60°C which was necessary for the P2SM. This optic used four elements, two of which could act as windows to the mask and a third could be the dewar window, the fourth element would also be the window at the front. The field of view can be increased by combining these modules and a large field of view system was considered using a 3x3 array of these WFOV optical modules. It was assumed that x4 super-resolution could be achieved in x and y using ACAI. The second design was for a narrow FOV optic which could achieve the necessary resolution directly but over a much smaller FOV, figure 14b. The design approach adopted was a very simple six element athermalized, refractive/diffractive design, this resulted in an optic that was 140cm long. Shorter designs would be optically more complex and would probably increase the optics count and hence the overall mass. As a result of the reduced FOV of this design a 12x12 array of these NFOV optical modules would be needed to achieve the required total FOV of the system.

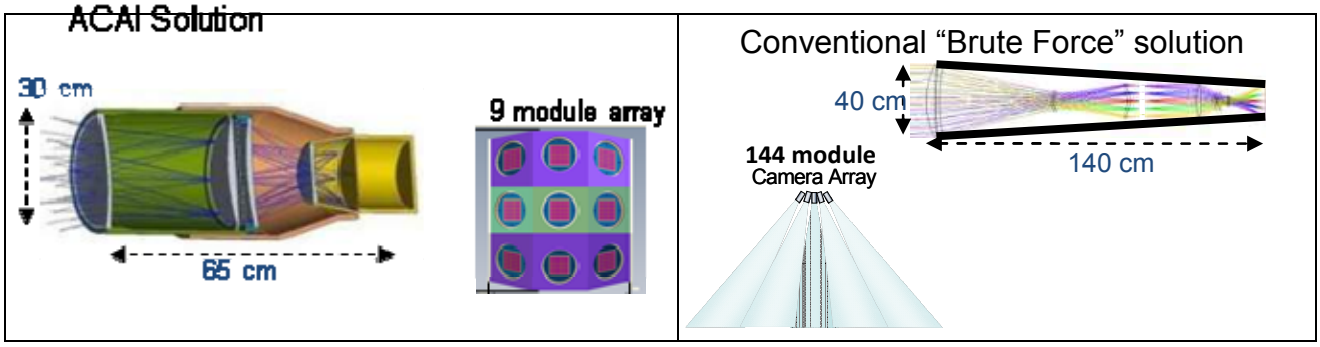


Figure 14 (a) outline design of the WFOV optic suitable for one module of the ACAI solution for PWAS (b) outline design of NFOV optic suitable for a conventional approach to this requirement

Comparisons of the size and weight of the total sensor configuration to achieve the PWAS requirement are shown in table 2. It can be seen that the system based on ACAI is over an order of magnitude smaller and lighter than the conventional approach, whose size and weight make it completely impractical.

| | **ACAI** | **Conventional (refractive/diffractive)** |
|---|---|---|
| Module count | 9 | 144 |
| System mass /kg | 350 | 10 000 |
| System volume / m3 | 0.75 | 29 |
| Data generation rate (@ 10 fps) / pixels $s^{-1}$ | $3.24 \times 10^{9}$ | $5.2 \times 10^{10}$ |
| FPA operability O required for tracking | *O>95%* | *O*>99.5% |
| Optics complexity | Simpler | More complex |
| System relative cost | 1 | 10 |
| Post detection beam forming | Yes | No |

Table 2. Comparisons between and ACAI and conventional approach to a PWAS requirement.

The ACAI approach also has much lower data rate, can tolerate FPAs with larger percentage of dead or out of range pixels, has simpler optics and would be an order of magnitude cheaper. Another benefit of the ACAI approach is that it will enable the data collected to be processed in different ways after collection – post detection beam forming – which would allow the extraction of different information.

Other relatively conventional approaches were also considered, these included step-stare and combined WFOV coupled to steerable NFOV. Estimates of size and weight were made for both these approaches based on the WFOV and NFOV optical designs described above. A large steering mechanism would also be required for both of these alternative approaches. Besides significant size and weight penalties with these approaches compared with the ACAI approach there were also other downsides, e.g. the step-stare would take several 10's seconds to complete a cycle which would make reliable tracking impossible.

## 6. CONCLUSIONS AND WAY FORWARD

Terrestrial imaging and tracking trials of an adaptive coded aperture demonstrator operating in the MWIR have been carried out, supported by a comprehensive system model. These have produced results confirming some of the potential of this computational imaging approach.

Immediate technology next-steps for refinement of this particular embodiment of MWIR ACAI could include engineering optimization of the FPA cooling technique to improve FPA mechanical stability. Ultimate performance could also be enhanced by characterization and minimization of crosstalk in the FPA by appropriate device design.

For application of this technology in persistent surveillance, the next important step in development must be airborne trials of a demonstrator – terrestrial trials can only go so far, and are no substitute for operation of the system in its desired look-down orientation. Subsequent developments could include fuller system trade analyses and optimization of decoding algorithms and subsequent DSP implementations for specific application requirements e.g. those of a PWAS system.

Finally, it is worth observing that this paper has described and verified only some aspects of ACAI. Other merits of the technology that have not so far been exploited e.g. innate multispectral and polarimetric capabilities, lens free imaging, imaging through ogives, now deserve attention. As do other applications: space based tracking, missile seekers, low cost man portable imagers, tactical imagers for UAVs and dismount tracking are all now in a position to be explored with some confidence. The ACAI approach offers similar order of magnitude performance improvements in meeting these, and other demanding, military and commercial needs.

## ACKNOLWLEDGEMENTS

The authors would like to acknowledge support from Phil Giguere and the wider Goodrich Team (Goodrich ISR Systems); Web Stayman (MTRI); Peter Roberts, Michael Gray, Darrel Heuchert, Frank Jaworski, Mark Luke (Raytheon Vision Systems); Phil Rogers (VNF Optic) for the WFOV and NFOV optical designs; the extended QinetiQ project and technical teams, including Simon Bray, Steve Kerry, and Andrew McClelland.

## REFERENCES

1. Dicke, R.H. “Scatter-hole cameras for X-rays and Gamma-rays,” The Astrophysical Journal 153, L101-L106 (1968).
2. Cannon T.M. and Fenimore, E.E., “Coded aperture imaging: many holes make light work”, Opt Eng 19, p.283-289 (1980).
3. Sanchez, F., Chato, R., Gasent, J. L., Rodrigo, J. and Velasco, T., “A coded mask for γ -ray astronomy. Design and calibration,” Nuclear Instruments and Methods in Physics Research A 500, p.253-262 (2003).
4. Barthelmy, S.D., Barbier, L.M., Cummings, J.R., Fenimore, E.E., Gehrels, N., Hullinger, D., Krimm, H.A., Markwardt, C.B., Palmer, D.M.. Parsons, A., Sato, G., Suzuki, M., Takahashi, T., Tashiro, M. and Tueller, J. “The Burst Alert Telescope (BAT) on the Swift MIDEX Mission,” Space Science Reviews, 120, p.143–164 (2005).
5. Brady D.J., “Optical Imaging and Spectroscopy”, ISBN: 9780470048238, Wiley-Blackwell (29 April 2009).
6. Slinger, C., Eismann, M., Gordon, N., Lewis, K., McDonald, G., McNie, M., Payne, D., Ridley, K., Strens, M., De Villiers, G. and Wilson, R., “An investigation of the potential for the use of a high resolution adaptive coded aperture system in the mid-wave infrared,” Proc. SPIE Vol. 6714, 67140 (2007).

7. Ridley, K.D., De Villiers, G.D., Payne, D.A., Wilson, R.A. and Slinger, C.W., "Visible band lens-free imaging using coded aperture techniques," Proc. SPIE 7468, 746809 (2009).
8. Space News International **20**, 11 (2009).
9. De Villiers, G.D., Gordon, N.T., Payne, D.A., Proudler, I.K., Skidmore, I.D., Ridley, K.D., Bennett, C.R., Wilson, R.A., Slinger, C.W., "Sub-pixel super-resolution by decoding frames from a reconfigurable coded-aperture camera: theory and experimental verification", Proc. SPIE 7468, (2009).
10. Chi, W. and George, N., "Phase-coded aperture for optical imaging", Optics Communications 282, p.2110–2117, (2009).
11. Veeraraghavan, A., Raskar, R., Agrawal, A., Mohan, A., and Tumblin, J., "Dappled Photography: Mask Enhanced Cameras for Heterodyned Light Fields and Coded Aperture Refocusing", ACM Transactions on Graphics (TOG), ISSN: 0730-0301, Vol. 26, Issue 3, Article 69, Jul. 2007.
12. Bertero, M. and Boccacci, P., Introduction to Inverse Problems in Imaging, IOP Publishing Limited, Bristol (1998).
13. Stayman J.W., Subotic N. and Buller W., "An analysis of coded aperture acquisition and reconstruction using multi-frame code sequences for relaxed optical design constraints", Proc. SPIE 7468, 74680D (2009).
14. Article in Space News International, Vol.20, Issue 33, p.11, 24 Aug. 2009.
15. McNie, M.E., Combes, D.J., Smith, G.W., Price, N., Ridley, K.D., Brunson, K.M., Lewis, K.L., Slinger, C.W. and Rogers, S., "Reconfigurable mask for adaptive coded aperture imaging (ACAI) based on an addressable MOEMS microshutter array," Proc. SPIE Vol. 6714, 67140B, (2007).
16. Huckridge, D., Bennett, C., Ridley, K., Slinger, C., Rogers, P. and Rice, K., "Coded aperture system performance comparison with conventional optics based approaches," Proc. SPIE Vol. 7818, 78180A, (2010).
17. Slinger, C., Gordon, N., Lewis, K., McDonald, G., McNie, M., Payne, D., Ridley, K., Strens, M., De Villiers, G. and Wilson, R., "Coded aperture systems as nonconventional, lensless imagers for the visible and infrared," Proc. SPIE Vol. 6737, 67370D, (2007).
18. McNie, M.E., Scott, A.M., Price, N., Combes, D.J., Smith, G.W., Ridley, K.D., Brunson, K.M., Jones, D.C., Lewis, K.L., "Large area transmissive modulator for a remotely-interrogated MEMS-based optical tag," Proc. SPIE Vol. 7208, 720806, (2009).
19. Gordon, N.T., De Villiers, G.D., Ridley, K.D., Bennett, C.R., McNie, M.E., Proudler, I.K., Russell, L., Slinger, C.W., and Gilholm, K., "An experimental infrared sensor using adaptive coded apertures for enhanced resolution," Proc. SPIE Vol. 7818, 781806, (2010).
20. Gilholm, K., Slinger, C.W., Gordon, N.T., Ridley, K., Bennett, C.R. and McNie, M.E. "Tracking point targets at sub-pixel accuracy in adaptive coded aperture imagery without decoding," Proc. SPIE Vol. 7818, 781808, (2010).
21. Bennett, C.R., Ridley, K.D., De Villiers, G.D., Watson, P.J., Slinger, C.W., and Rogers, P.J., "Optical design of a coded aperture infrared imaging system with resolution below the pixel limit," Proc. SPIE Vol. 7818, 78180H, (2010).
22. McNie, M.E., Brown, A.G., King, D.O., Smith, G.W., Gordon, N.T., Riches, S. and Rogers, S., "A 2x2 multi-chip reconfigurable MOEMS mask: a stepping stone to large format microshutter arrays for coded aperture applications ", SPIE-7818A, Invited paper – Proc. SPIE Vol. 7818, 78180G, (2010).
23. McNie, M.E., Davies, R.R., Johnson, Al, Hardy, B., Hames, G., Monk, D., Rogers, S., SPIE 8165b-50, (2011).